Historical and near-real time SST retrievals from MetOp AVHRR FRAC with the advanced clear-sky processor for ocean

Pryamitsyn, V., Petrenko, B., Ignatov, A., Jonasson, O., Kihai, Y.

V. Pryamitsyn, B. Petrenko, A. Ignatov, O. Jonasson, Y. Kihai, "Historical and near-real time SST retrievals from MetOp AVHRR FRAC with the advanced clear-sky processor for ocean," Proc. SPIE 11752, Ocean Sensing and Monitoring XIII, 1175204 (12 April 2021); doi: 10.1117/12.2585893

SPIE.

Event: SPIE Defense + Commercial Sensing, 2021, Online Only

Historical and Near-real Time SST retrievals from Metop AVHRR FRAC with the Advanced Clear-Sky Processor for Ocean

V. Pryamitsyn[1, 2], B. Petrenko[1, 2], A. Ignatov[1], O. Jonasson[1, 2], Y. Kihai[1, 2]
[1]NOAA STAR, [2]GST, Inc.

ABSTRACT

The first full-mission AVHRR FRAC SST dataset with nominal 1.1km resolution at nadir was created from three Metop First Generation (FG) satellites: A (2006-present), B (2012-present) and C (2018-present), using the NOAA Advanced Clear-Sky Processor for Ocean (ACSPO) enterprise system. Historical reprocessing (Reanalysis-1, RAN1) starts at the beginning of each mission and continues into near-real time (NRT) processing. ACSPO generates two SST products: Global Regression (GR) SST, highly sensitive to the skin SST, and Piecewise Regression (PWR) SST, a proxy for the depth SST. The effect of orbital and sensor drift on the stability of the SST time series is mitigated by retraining the regression coefficients daily against matchups with the drifting and tropical moored buoys. Those matchups are collected within moving windows: 91-day for GR and 361-day for PWR, with the offsets adjusted within a 31 day window. In RAN1, all training and offset correction windows are centered at the processed day. In NRT processing, the training and offset delayed windows of the same sizes and ending in 4-10 days prior to the processed day are used. This mitigates long-term calibration trends on scales from 1-2 months in both RAN1 and NRT. Short-term variations in SST biases in NRT are higher than in RAN1 but do not exceed ~0.05 K. Delayed-mode RAN processing follows the NRT with a lag of ~2 months, resulting in higher quality, more consistent Metop-FG SST record. The presentation evaluates the performance of the ACSPO AVHRR FRAC dataset and compares it with the EUMETSAT OSISAF Metop-A and -B FRAC SSTs available in PO.DAAC.

Keywords: Metop FRAC, SST, reanalysis

1. INTRODUCTION

The AVHRR/3 data in a Global Full Resolution Area Coverage (FRAC) mode (resolution 1.1 km at nadir degrading to ~6 km at swath edge) has been available since the launch of Metop-A on 19 October 2006, followed by Metop-B (17 September 2012) and Metop-C (November 7, 2018). Together, these three satellites comprise the Meteosat First Generation (FG) series. Although global FRAC data are well suited for superior cloud masking and high quality sea surface temperature (SST) retrievals (from AVHRR bands 3b, 4 and 5 centered at 3.7, 10.8 and 12 μm), no complete record from Metop-FG existed up until now.

The first full record of Metop AVHRR FRAC SSTs has been created at NOAA with its enterprise Advanced Clear-Sky Processor for Oceans system [1-5]. Historical reprocessing (RAN1) starts after quality AVHRR L1b data in the infrared bands became available (1 December 2006 for Metop-A, 19 October 2012 for Metop-B, and 4 December 2018 for Metop-C) and is supplemented with the near-real time (NRT) processing, with several hours latency. Retrieved SSTs are available in L2P, L3U and L3S [6] formats. Presently, the data are stored in NESDIS/STAR local storage, and the archival with the Physical Oceanography Distributed Active Archive Center (PO.DAAC) [7-12] and NOAA Centers for Environmental Information (NCEI) is underway.

This study documents the performance of the ACSPO AVHRR FRAC L2P SST, by analyzing time series of biases and standard deviations of retrieved SSTs minus quality controlled *in situ* SSTs (SQUAM, [13, 14]). The *in situ* SSTs from drifting and tropical moored buoys and from Argo floats are obtained from another NOAA system, *in situ* Quality Monitor (*i*Quam, [15, 16]. We also show the time series of clear-sky fractions (percent of SST pixels to the total ice-free ocean pixels) in a manner similar how it was done in the prior AVHRR GAC RAN1 and RAN2 analyses [2, 17, 18].

[1]Email: victor.pryamitsyn@noaa.gov; Phone: +1-301-683-3366

Ocean Sensing and Monitoring XIII, edited by Weilin "Will" Hou, Proc. of SPIE Vol. 11752,
1175204 · © 2021 SPIE · CCC code: 0277-786X/21/$21 · doi: 10.1117/12.2585893

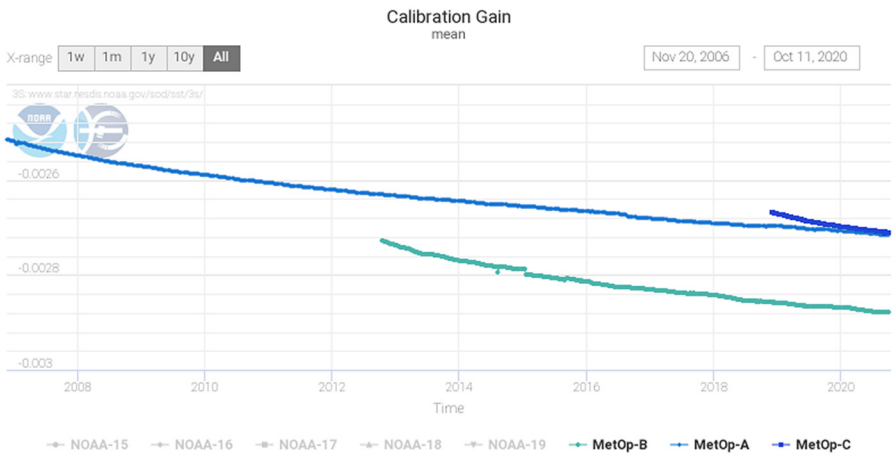

Figure 1 Metop AVHRR Calibration Gains in channel 3B degrade in time [19, 20]. Although the L1b calibration algorithm should account for these degradations, the likelihood of systematic residuals remains. The utilization of the variable coefficients help mitigate the effect of such sensor degradation on SST.

2. ACSPO AVHRR FRAC SST ALGORITHMS AND PRODUCTS

The cloud filtering in ACSPO is performed with the ACSPO Clear-Sky mask [1] which employs a set of threshold-based filters. ACSPO SST retrieval and training algorithms, employed in the AVHRR FRAC RAN1 and NRT processing, are similar to those used in the AVHRR GAC RAN2 [17, 18]. Here we only briefly summarize their main features. ACSPO generates two SST products: the Global Regression (GR, or 'subskin') and the Piecewise Regression (PWR; proxy for 'depth') SSTs. The GR SST is more sensitive to skin SST, although it is anchored to *in situ* 'depth' SST. The PWR SST is also referred to as 'debiased' SST, because it is calculated as a difference between the two data layers reported in the ACSPO files, the GR SST and the Single Sensor Error Statistics (SSES) bias. The PWR SST is less sensitive to skin SST but more accurate and precise with respect to *in situ* SST [3]. In contrast to the GR SST, produced with one global set of regression coefficients, the PWR SST is produced with multiple sets of regression coefficients, selected depending on the values of the regressors. Each set of PWR coefficients is trained against a specific subset of global matchups [3]. The SST algorithm employs three AVHRR bands 3b (3.7 μm), 4 (10.8 μm) and 5 (12 μm) at night and two bands, 4 and 5, during the day. The day- and nighttime algorithms are switched at solar zenith angle 90°. The first guess SST for NLSST retrievals is obtained from the L4 SST by the Canadian Meteorological Center (CMC, v1 with 0.2° resolution before Dec 2016 and v2 with 0.1° resolution after January 2017). The regression coefficients are trained using matchups with drifting and moored buoys, available from the NOAA *i*Quam system [15, 16], To compensate for calibration and orbital drifts, the regression coefficients are retrained daily using matchups within moving windows, 91-day for GR SST and 361-day for PWR SST. The offsets of equations are additionally adjusted using moving windows of 31-day size. In RAN, those windows are centered at the processed day. The NRT processing uses delayed windows of the same size, but ending ~4-10 days prior to the processed day (depending on matchups' availability), with offsets adjusted from the last 31 days in each training window.

The main reason for employing variable regression coefficients is the need for mitigating the AVHRR calibration trends [19]. Figure 1 illustrates these trends with the time series of gain in the Metop AVHRR channel 3b. Although the L1b calibration algorithm is supposed to account for such degradation, the systematic residuals still take place. Using variable regression coefficients helps mitigate the effect of such sensor degradation on SST. Another factor contributing to the unstable BTs is orbital drift (See Figure 2). Note also that Metop orbits are periodically corrected to maintain the 9:30am/pm local equator crossing time, but nevertheless, small residual trends in SST due to changing overpass time may still remain. Moreover, the Metop-A orbit has not been controlled since Sep 2016, which increases the need for variable regression coefficients (although it may not be fully sufficient).

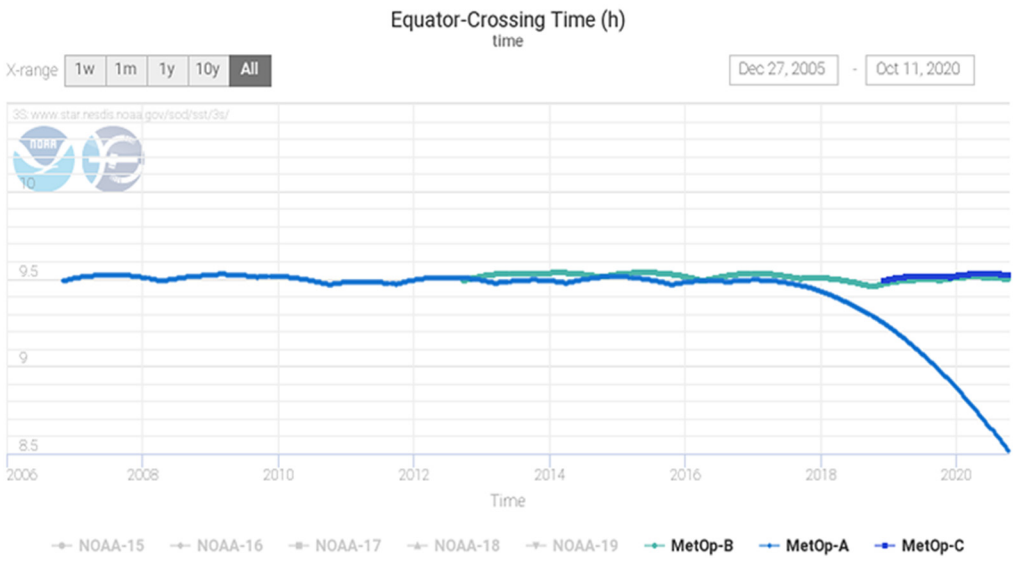

Figure 2. Variations in the equator crossing time of Metop-A, Metop-B and Metop-C [19, 20].

3. EUMETSAT OSISAF METOP FRAC SST DATA SET

To place the newly created ACSPO AVHRR FRAC SST dataset in context, we compare it with the only available up until recently AVHRR FRAC SST dataset, produced by EUMETSAT OSISAF and available from two PO.DAAC datasets: "AVHRR_SST_METOP_A-OSISAF-L2P-v1.0", which covers the period from 06/04/2013 to 11/23/2016 [21], and "AVHRR_SST_METOP_B-OSISAF-L2P-v1.0" for the period 01/19/2016 to present [22]. The SST data set of Metop-C, launched in November 2018, is not yet available. Following the GDS-2 standard, and similarly to the ACSPO SST dataset, the OSISAF data sets provides 'subskin' SST and SSES bias layers, which allow estimation of 'debiased' SST by subtracting SSES bias from the 'subskin' SST. In this presentation, we compare the performances of both 'subskin' and 'debiased' products from the ACSPO and OSISAF data sets. This presentation uses quality levels 3, 4 and 5 as recommended by OSISAF [23]. The OSISAF uses different SST retrieval algorithms for daytime and nighttime SSTs: two-band regression when SZA <90°; three-band regression when SZA >110°, and a combination of 2- & 3-band algorithms in twilight zone [24, 25]. Angular terms and offsets are adjusted from matchups with *in situ* data. Note that Metop-A and -B algorithms are different. Regression SSTs for Metop-B are additionally corrected for bias using the RTM-based algorithm [26, 27]. In this paper, performance of the ACSPO SST is placed in context of OSISAF SST, only for nighttime SSTs. The daytime statistics are provided for ACSPO SST only. The validation statistics for the daytime OSISAF SST can be found in SQUAM [14] and in the SPIE presentation associated with this paper.

4. VALIDATION

We consistently validate satellite SSTs against *in situ* data from drifting and tropical moored buoys (D+TM) and Argo floats (AF) form the NOAA *i*Quam system [15, 16]. Both D+TM and AFs use one-to-many matchups within the (10km×30min) window.

Consistency checks against Level 4 (L4) employs Canadian Meteorological Center (CMC) L4 SST (v1 0.2° before Dec 2016, and v2 0.1° after Jan 2017) [28, 29]. Results of both validation against *in situ* data and consistency checks against L4 are published in the NOAA SQUAM system [14]. This report presents the results for both nighttime and daytime SSTs. More complete results are available in SQUAM [14].

4.1 Geographical distributions of matchups

Figure 3 shows examples of nighttime monthly aggregated maps of 'subskin' – (D+TM) SST and 'subskin' – AF SST for July 2016. Coverage by Matchups with *i*Quam (D+TM) is nearly uniform & globally representative, for both products. The latter is also true for matchups with AFs, although they are two orders of magnitude sparser than with (D+TM).

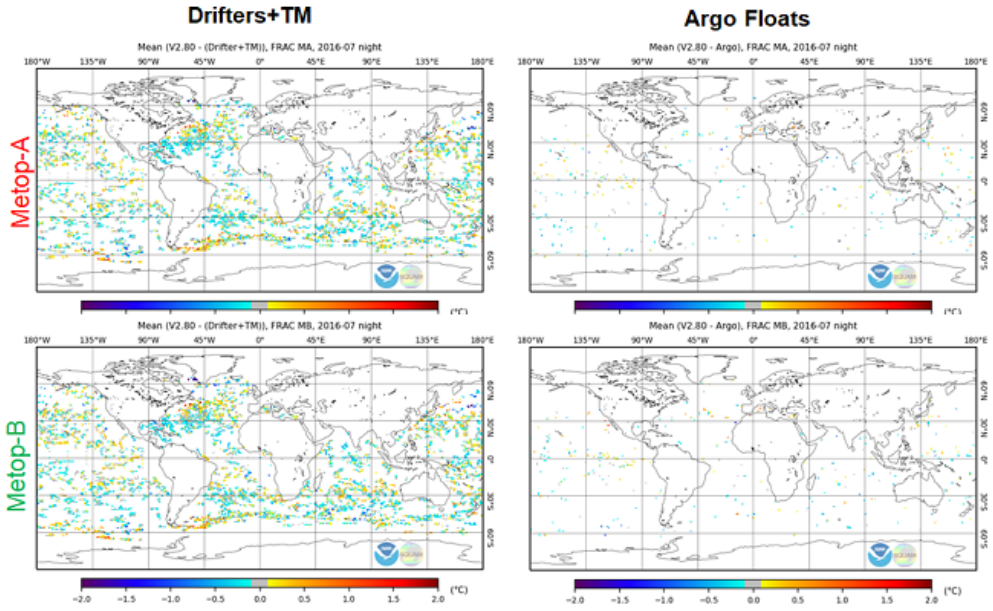

Figure 3 Nighttime monthly aggregated maps of (left panels) 'subskin' – (D+TM) SST and (right panels) 'subskin' – AF SST, produced from (upper panels) Metop-A and (bottom panels) Metop-B for July 2016.

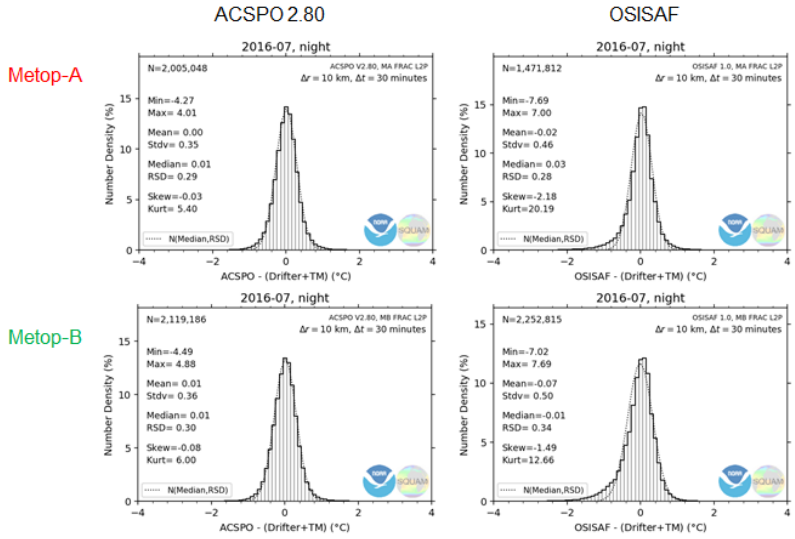

Figure 4. Monthly histograms of nighttime (left panels) ACSPO 'subskin' – (D+TM) SST and (right panels) OSISAF 'subskin' – (D+TM) SST, produced from (upper panels) Metop-A and (bottom panels) Metop-B.

4.2 Monthly histograms of satellite – (D+TM) SSTs

Figure 4 shows monthly histograms of nighttime 'subskin' – (D+TM) SSTs. In ACSPO, the number of matchups and validation statistics are consistent between Metop-A and -B. In OSISAF product, Metop-B coverage is comparable with ACSPO and larger than for Metop-A (recall that OSISAF employed different algorithms for Metop-A and -B). For both satellites, ACSPO validation statistics improve relative to OSISAF. Note that cold tails in ACSPO histograms are minimal, suggesting reduced cloud leakages. This is discussed in more detail in section 5.

Figure 5 shows monthly histograms of 'debiased' – (D+TM) SST's. The debiasing in ACSPO significantly reduces SDs with respect to *in situ* SST, which is not the case for the OSISAF 'debiased' SST.

The monthly histograms of daytime ‘subskin’ and ‘debiased’ minus (D+TM) SSTs are shown in Figure 6 and Figure 7, respectively. As expected, in both data sets, daytime SDs are higher compared to their nighttime counterparts. The daytime ACSPO statistics for all three Metop-FG remain consistent, with SDs for ‘debiased’ SSTs being significantly lower than for ‘subskin’ SSTs.

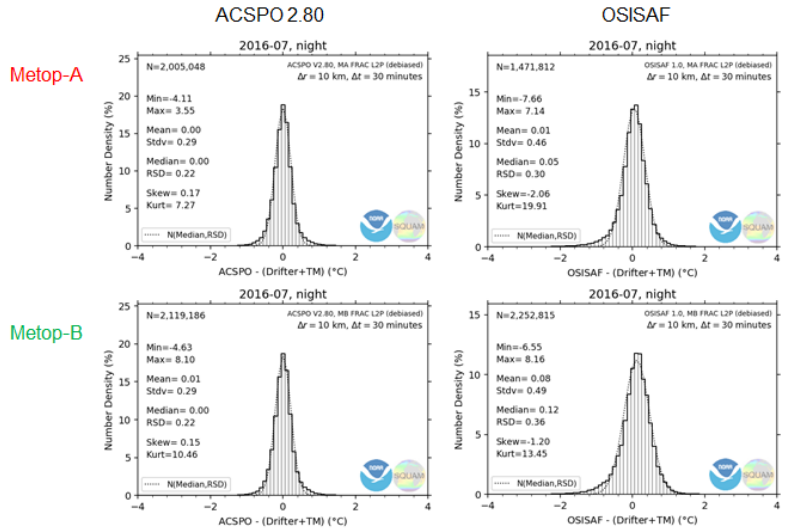

Figure 5 Monthly histograms of nighttime (left panels) ACSPO ‘debiased’– (D+TM) SST and (right panels) OSISAF ‘debiased’ – (D+TM) SST, produced from (upper panels) Metop-A and (bottom panels) Metop-B.

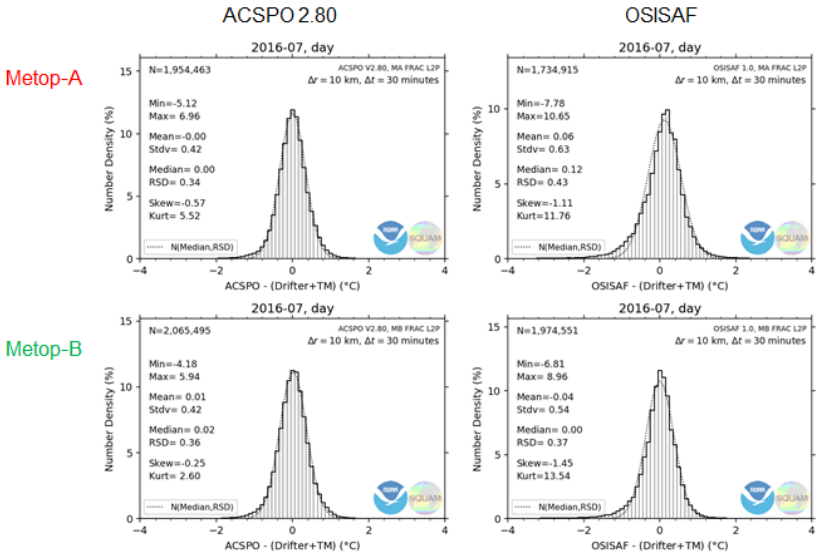

Figure 6. Monthly histograms of daytime (left panels) ACSPO ‘subskin’ – (D+TM) SST and (right panels) OSISAF ‘subskin’– (D+TM) SST, produced from (upper panels) Metop-A and (bottom panels) Metop-B.

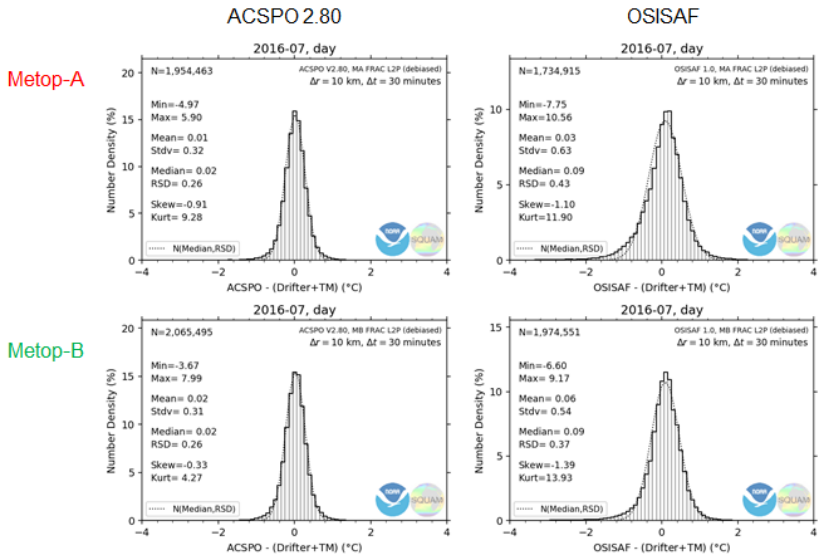

Figure 7. Monthly histograms of daytime (left panels) ACSPO 'subskin'– (D+TM) SST and (right panels) OSISAF 'subskin'– (D+TM) SST, produced from (upper panels) Metop-A and (bottom panels) Metop-B.

4.3 Time series of statistics with respect to (Drifters + Tropical Moorings)

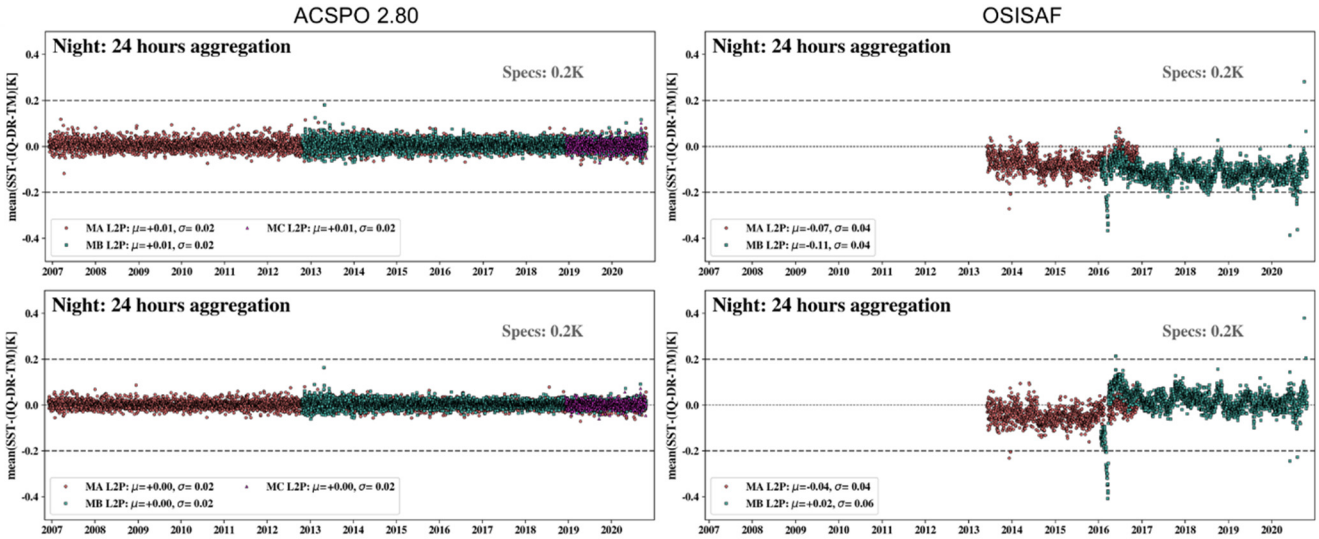

Figure 8. Time series of monthly biases of (top panels) 'subskin' and (bottom panels) 'debiased' SSTs wrt. (D+TM), in (left panels) ACSPO and (right panels) OSISAF products.

Figure 8 shows full time series of daily nighttime biases in the ACSPO and the OSISAF SST products. The ACSPO SST biases are stable and meet the NOAA SST specs of ±0.2 K with a wide margin. This is the effect of daily recalculation of regression coefficients. OSISAF SST biases in OSISAF are slightly negative and more variable than in ACSPO, but, generally, also within the ±0.2K NOAA specs. OSISAF biases are somewhat larger for Metop-A than for Metop-B.

ACSPO 'debiased' SST is even more consistent with (D+TM), with biases being closer to zero and grouped tighter than for 'subskin' GR SST. Biases in OSISAF 'debiased' SST are closer to 0K than for 'subskin' SST (more so for Metop-B), and generally remain within the ±0.2K specs. For Metop-A, the OSISAF debiasing under-corrects, and for Metop-B over-corrects a little.

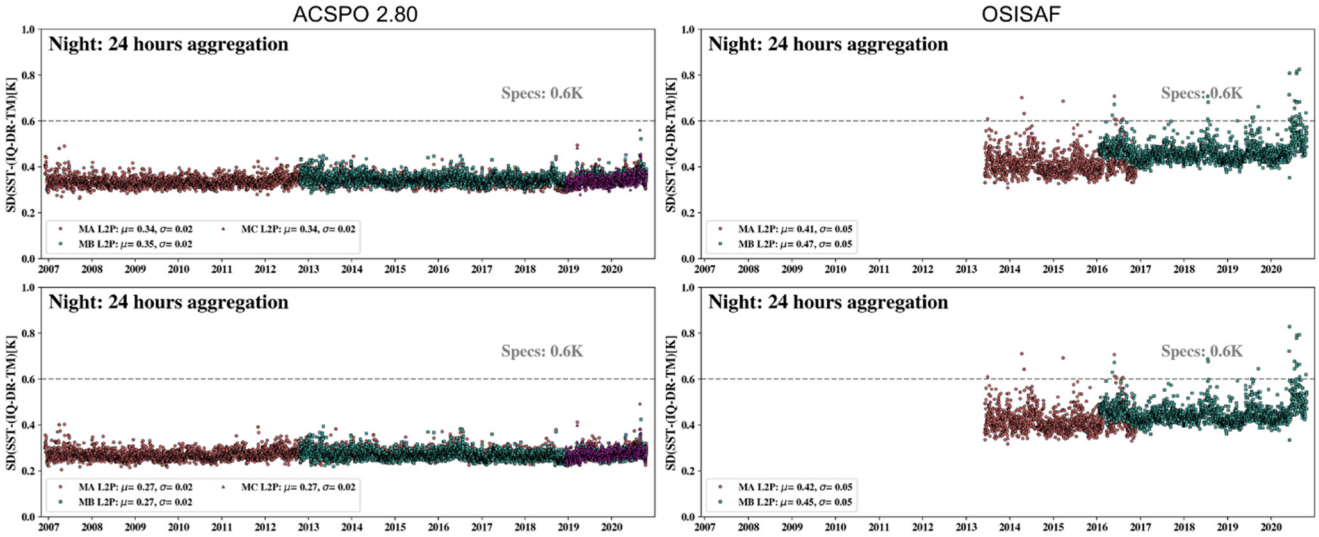

Figure 9. Time series of monthly standard deviations of (top panels) 'subskin' and 'debiased' SSTs wrt. (D+TM), in (left panels) ACSPO and (right panels) OSISAF products.

Figure 9 shows the time series of nighttime SDs with respect to (D+TM). The SDs in both ACSPO SSTs are consistent across all three satellites, and generally lower and more stable than in the corresponding OSISAF products. The SDs for ACSPO products meet the NOAA 0.6K spec by a wide margin. The OSISAF SSTs also mostly meet the NOAA specifications (by a somewhat wider margin for Metop-A, and narrower for Metop-B).

In ACSPO, the SDs for the 'debiased' SSTs are significantly lower than the SDs for the 'subskin' SST.

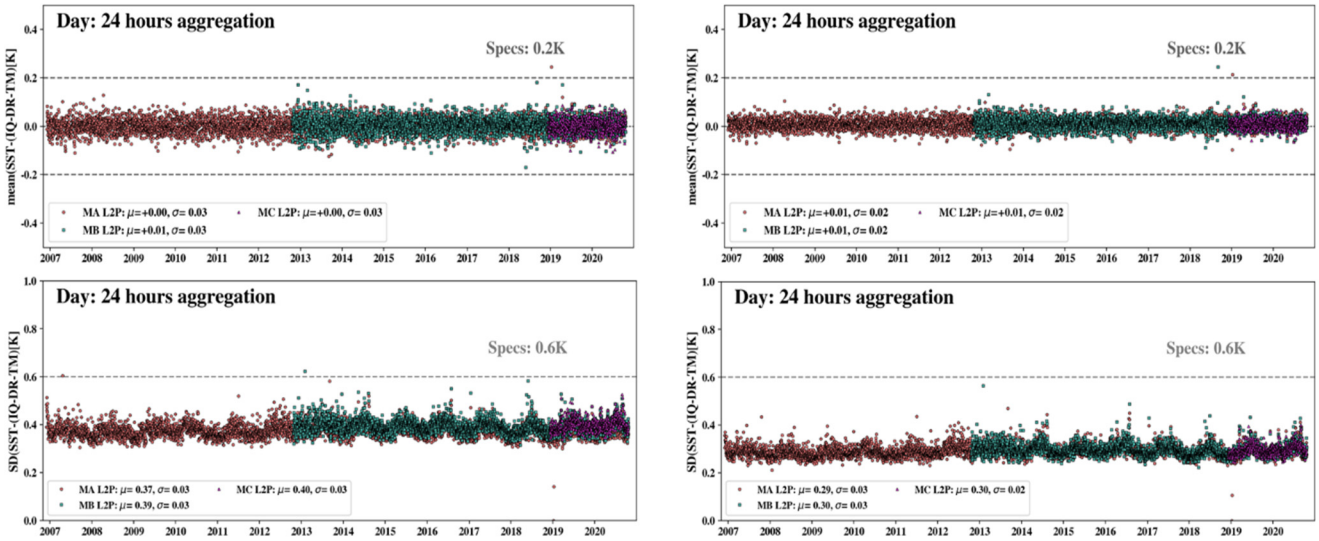

Figure 10. Time series of daytime monthly (top panels) biases and (bottom panels) SDs of ACSPO (left panels) 'subskin' SST and (right panels) ACSPO 'debiased' SST wrt. (D+TM).

Figure 10 shows the time series of statistics of daytime ACSPO 'subskin' and 'depth' SSTs with respect to (D+TM). The statistics are stable over the whole mission and consistent across three platforms. Generally, ACSPO SSTs meet NOAA specs with a wide margin. The daytime SDs show seasonality, likely due to systematic changes in diurnal warming pattern between the hemispheres, driven by seasonality of the insolation and wind speed. Biases in 'debiased' SST are closer to 0K and grouped tighter, with SDs noticeably lower than those of 'subskin' SST.

4.4 Independent validation against Argo Floats

Since the AFs were not used for training ACSPO and OSISAF SST algorithms, they represent an independent validation data set. Figure 11 compares monthly histograms and statistics of 'subskin'– AF SST for the ACSPO and OSISAF products. The ACSPO statistics are improved for both Metop-A and Metop-B over their OSISAF counterparts. Warm tail in all histograms is likely due to residual diurnal warming in satellite L2P SST at 9:30pm.

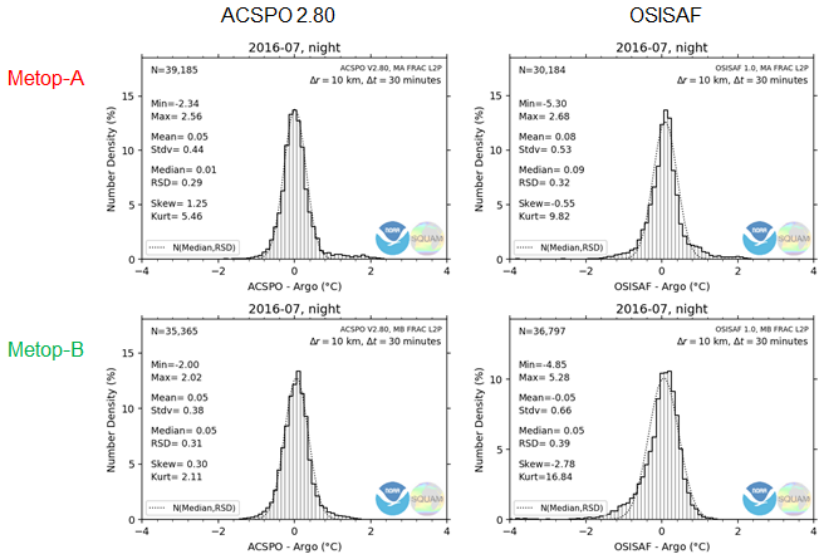

Figure 11. Monthly histograms of nighttime (left panels) ACSPO 'subskin'– AF SST and (right panels) OSISAF 'subskin' – AF SST, produced from (upper panels) Metop-A and (bottom panels) Metop-B.

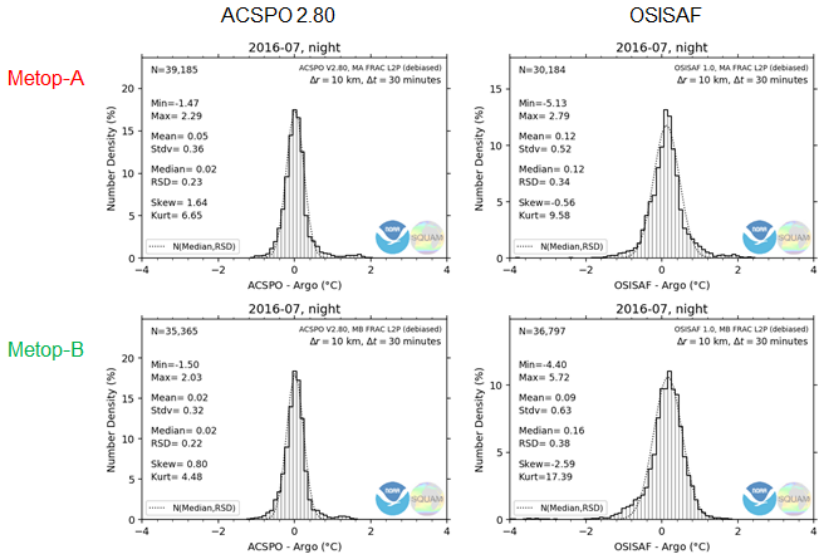

Figure 12. Monthly histograms of nighttime (left panels) ACSPO 'debiased' – AF SST and (right panels) OSISAF 'debiased' – AF SST, produced from (upper panels) Metop-A and (bottom panels) Metop-B.

Figure 12 compares the statistics and histograms for 'debiased' minus AF SST for ACSPO and OSISAF. As in the case of validation against (D+TM), the debiasing reduces global SDs for all products, and is more efficient in ACSPO.

Figure 13 shows monthly statistics for daytime Metop-A and -B ACSPO SST products. Both the coverage and SST statistics are consistent between Metop-A and -B.

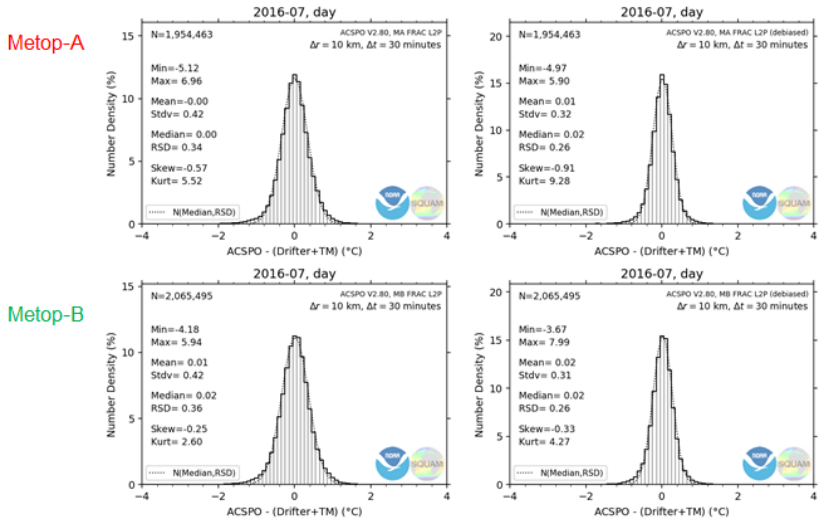

Figure 13. Monthly histograms of daytime (left panels) ACSPO 'subskin'– AF SST and (right panels) ACSPO 'debiased' – AF SST, produced from (upper panels) Metop-A and (bottom panels) Metop-B.

Figure 14 shows that biases in ACSPO– AF SST are relatively stable and consistent across Metop-A, -B and -C. (Recall that variable coefficients were calculated against the (D+TM), and fully independently of AFs).

ACSPO SST is slightly warmer than AFs, likely due to training against warmer (D+TM) at 0.2-1m depth (cf. ~6m depth for AFs). ACSPO biases are largely stable and well within the ±0.2K corridor. 'Debiased' ACSPO SST remains to be slightly warmer than AF, likely due to training against warmer (D+TM) at 0.2-1m depth.

OSISAF SST biases are also mostly within the ±0.2K corridor, and 'debiasing' largely reconciles Metop-A and -B SSTs. Both remain biased slightly warm wrt. AFs, for the same reason as in ACSPO.

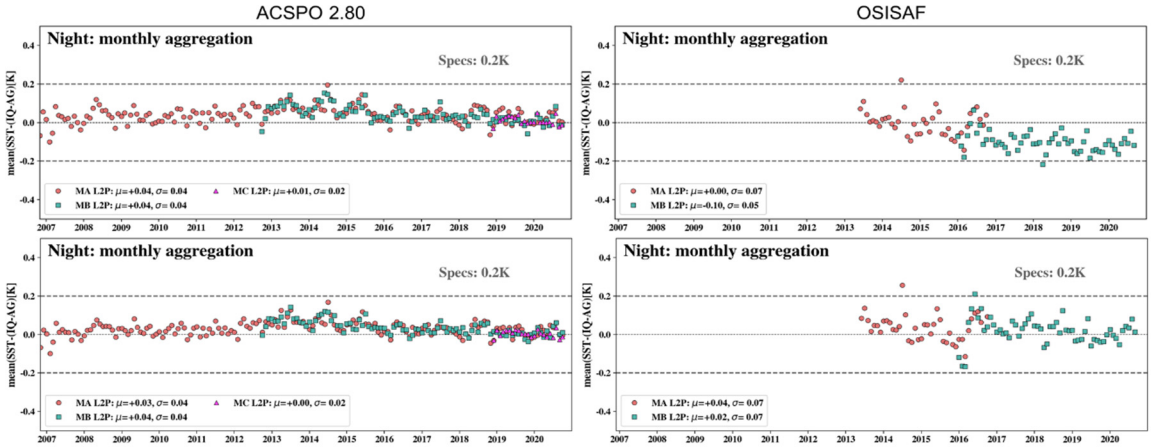

Figure 14. Time series of global monthly Biases of (top panels) 'subskin' (GR) and (bottom panels) 'debiased' – AF SSTs.

Figure 15 shows that, in ACSPO, Metop-A, -B and -C SDs wrt. AFs are consistent across three platforms. SDs wrt independent AFs (0.33-0.38K) are comparable to those wrt (D+TM) (0.32-0.35K), meeting NOAA specs by a wide margin. SDs in both datasets show seasonality, with SDs tending to be elevated during the NH Summer. In ACSPO, SDs of 'debiased' SST are reduced relative to 'subskin' (0.27-0.30K vs 0.33-0.38K), and consistent across all three platforms.

The SDs for OSISAF SSTs generally meet the NOAA 0.6K spec, and consistent between Metop-A and -B. SDs vs AFs (0.46-0.47K) remain close to the (D+TM) statistics (0.41-0.47K). The SDs tend to be elevated during the NH Summer (more so for Metop-A). OSISAF SSTs generally meet the NOAA 0.6K spec (more so for Metop-B than Metop-A). ACSPO SDs (0.27-0.30K) are improved relative to OSISAF SDs (0.45-0.46K).

Figure 16 shows the time series of daytime ACSPO biases and SDs of 'subskin' and 'debiased' wrt AF SSTs. The latter biases are relatively stable. As at night, daytime ACSPO SST tends to be slightly warmer than AF SST. ACSPO SDs are consistent across Metop-A, -B and -C (0.44-0.49K). In general, NOAA specs are met, except for a few boreal summer months. The SDs of ACSPO 'depth' SST are lower than for 'subskin' SST (0.34-0.36K vs 0.44-0.49K) and largely consistent across platforms, with well-pronounced seasonality for the daytime SST.

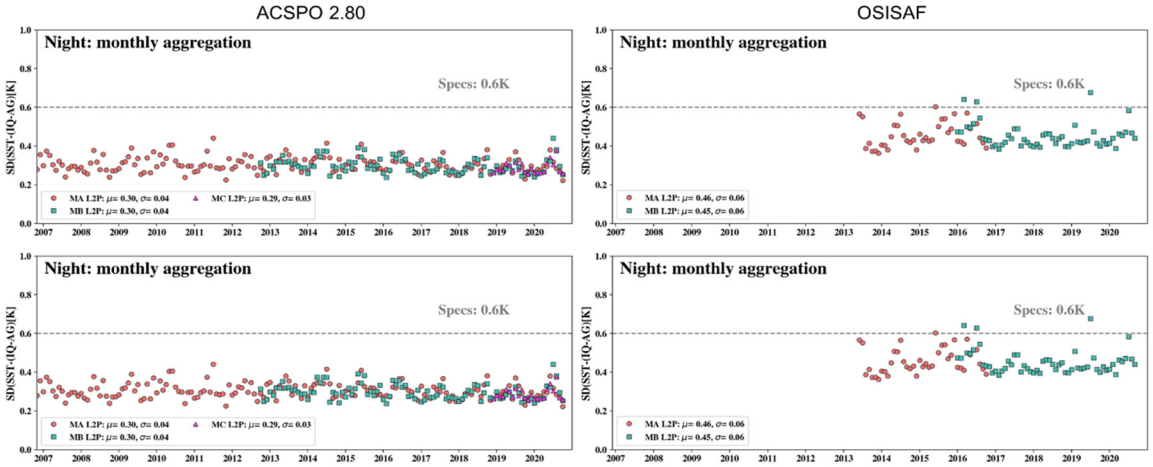

Figure 15. Time series of global monthly SDs of (top panels) 'subskin' GR SST and (bottom panels) 'debiased' – AF SST.

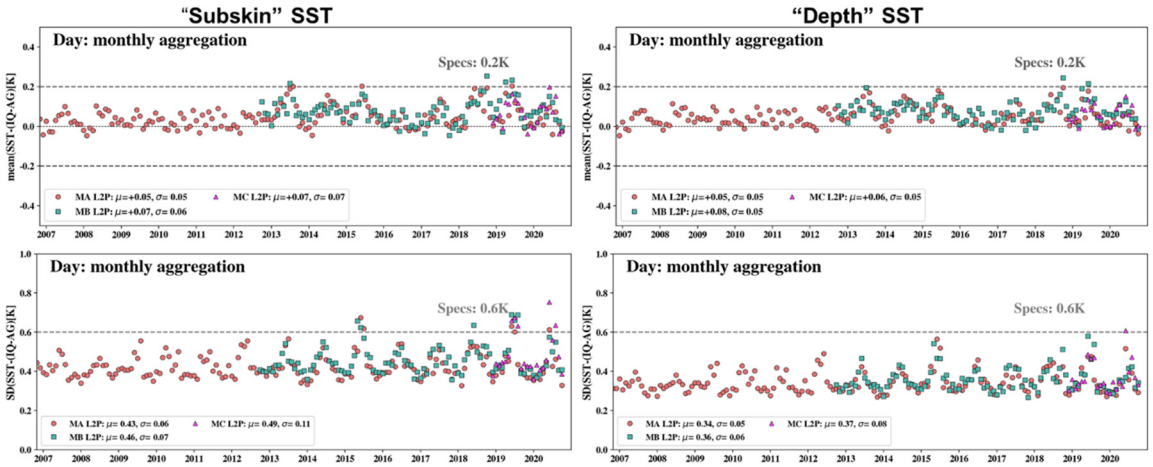

Figure 16. Daytime monthly (top panels) biases and (bottom panels) SDs of (left panels) 'subskin' (GR) and (right panels) 'depth' – AF SST.

5. NIGHTTIME CONSISTENCY CHECKS WITH CMC L4

Figure 17 shows composite maps of deviations of 'subskin' from CMC SST, produced from ACSPO and OSISAF data. Figure 18 shows similar maps but for 'debiased' SST. Both figures suggest that the cloud screening in ACSPO is more conservative than in OSISAF. The debiasing improves consistency between L2P SST & CMC L4 in both products, with ACSPO debiasing appearing more efficient.

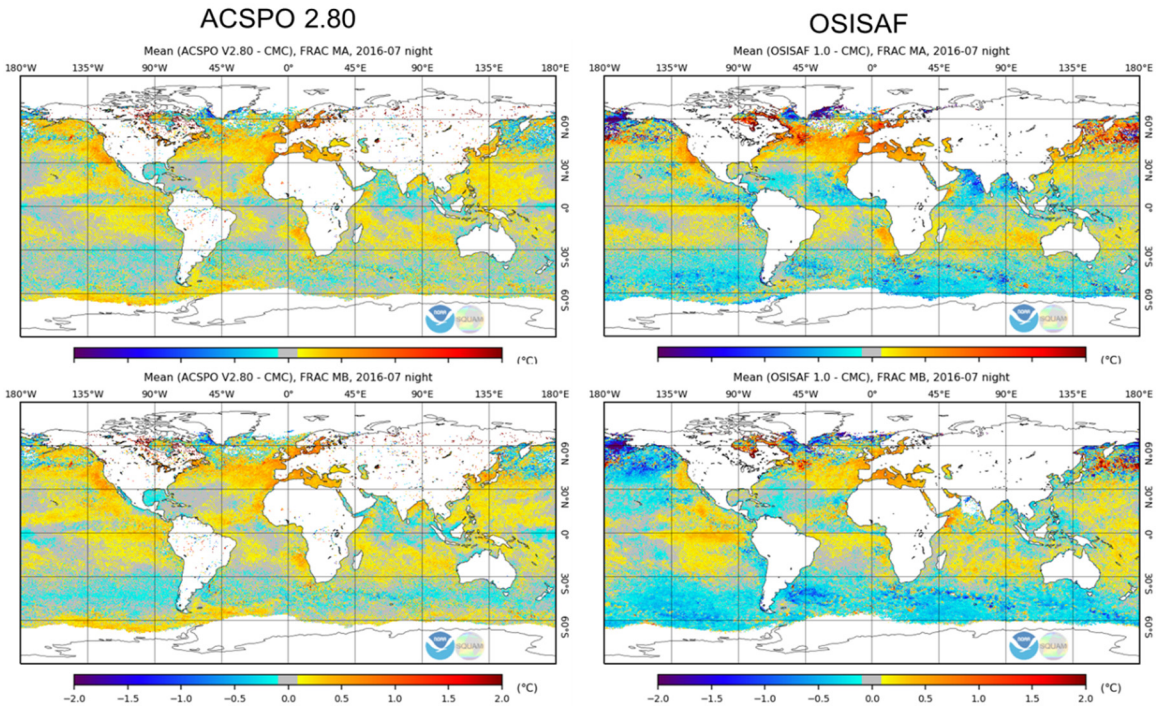

Figure 17. Nighttime monthly composite maps of 'subskin' – CMC SST for (top panels) Metop-A and (bottom panels) Metop-B, derived with (left panels) ACSPO and (right panels) OSISAF systems.

Figure 19 shows time series of nighttime biases of ACSPO and OSISAF SSTs wrt CMC SST. ACSPO SSTs are biased warm from ~+0 to +0.2K, consistently across all three platforms. Some seasonality is noticeable due to insolation/wind patterns. Metop-A starts deviating from once-a-day L4 SST in recent years due to its orbital shift from 9:30pm to 8:30pm.

The ACSPO 'debiased' SSTs remains biased warm wrt CMC (due to residual diurnal warming at 9:30pm). However, the scatter of daily biases is narrower than for 'subskin' SST and consistent across Metop-A, -B, sand -C platforms.

In OSISAF, the biases for Metop-A are more positive than for Metop-B. The offsets are noticeable during the Metop-A/B overlapping period. Similarly to ACSPO, the OSISAF SSTs show seasonality. The biases of the 'debiased' SST from Metop-B are centered closer to 0K, whereas for Metop-A, they are a little warmer. Metop-A and -B biases are not fully consistent during the overlapping period and less regular than in ACSPO.

Figure 20 shows the time series of nighttime SDs of 'subskin' SST and 'debiased' SST from CMC SST for the ACSPO and OSISAF datasets. In ACSPO, SDs of 'debiased' SST are much lower than those are for 'subskin' SST (0.25-0.27 K vs. 0.34-0.37 K), with both being consistent across the platforms. In OSISAF, the SDs are higher than in ACSPO. The SDs for Metop-A tend to be a little smaller than Metop-B. The seasonality is more pronounced in OSISAF SDs than in ACSPO SDs. In OSISAF, the margin between SDs for 'debiased' (0.46-0.47K) and 'subskin' (0.45-0.48K) SSTs is narrower than in ACSPO.

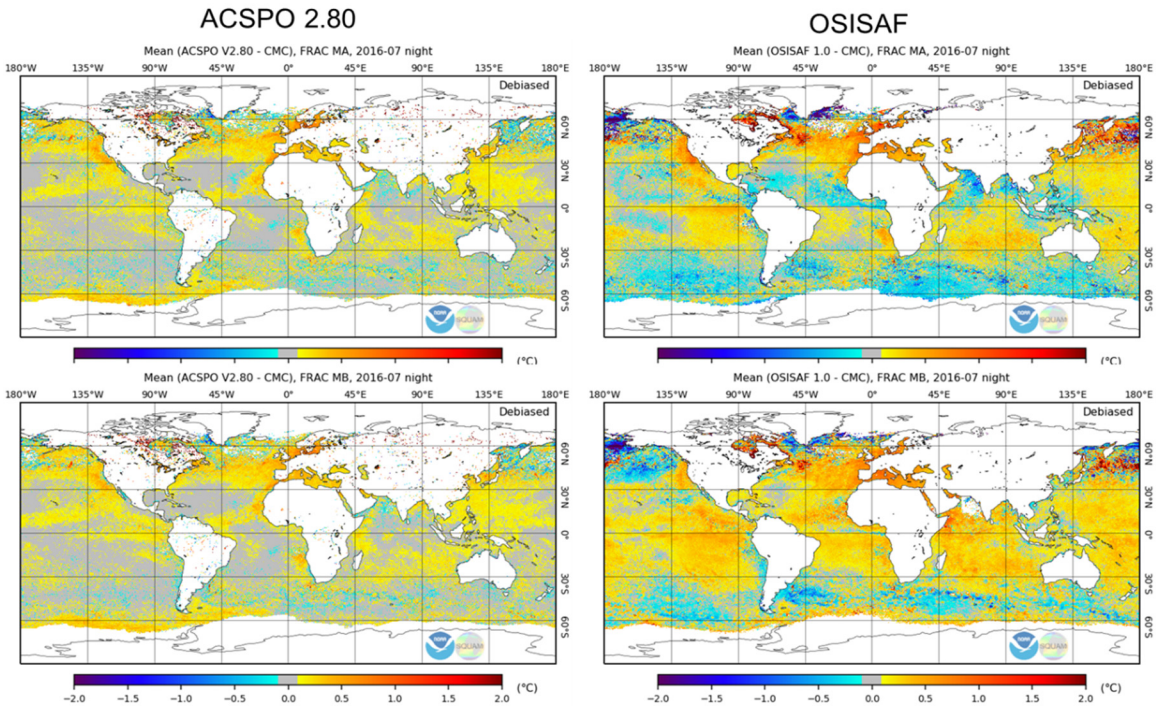

Figure 18. Nighttime monthly composite maps of 'debiased' – CMC SST from Metop-A (top panels) and Metop-B (bottom panels), produced from (left panels) ACSPO and (right panels) OSISAF data.

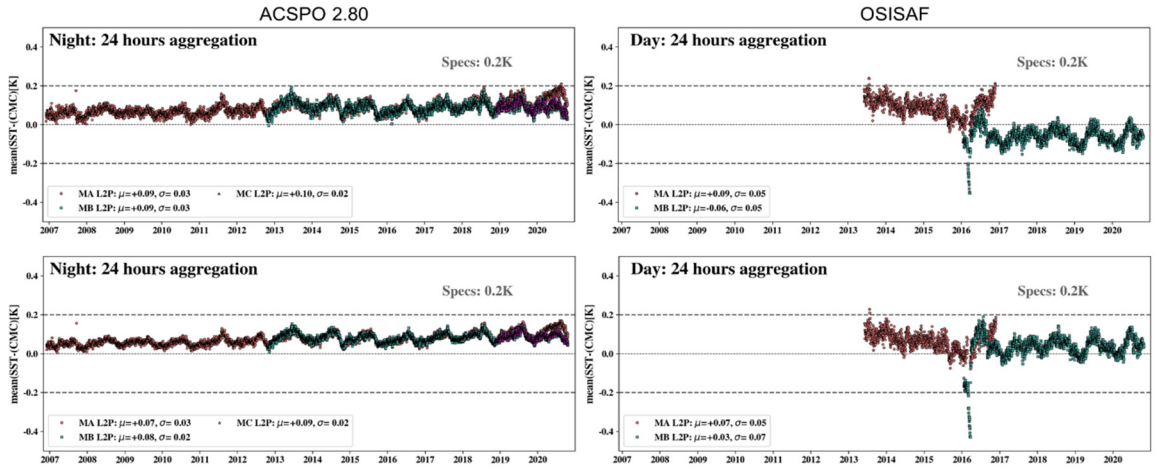

Figure 19. Time series of nighttime (top panels) biases and (bottom panels) standard deviations of 'subskin'– CMC L4 in (left panels) ACSPO and (right panels) OSISAF.

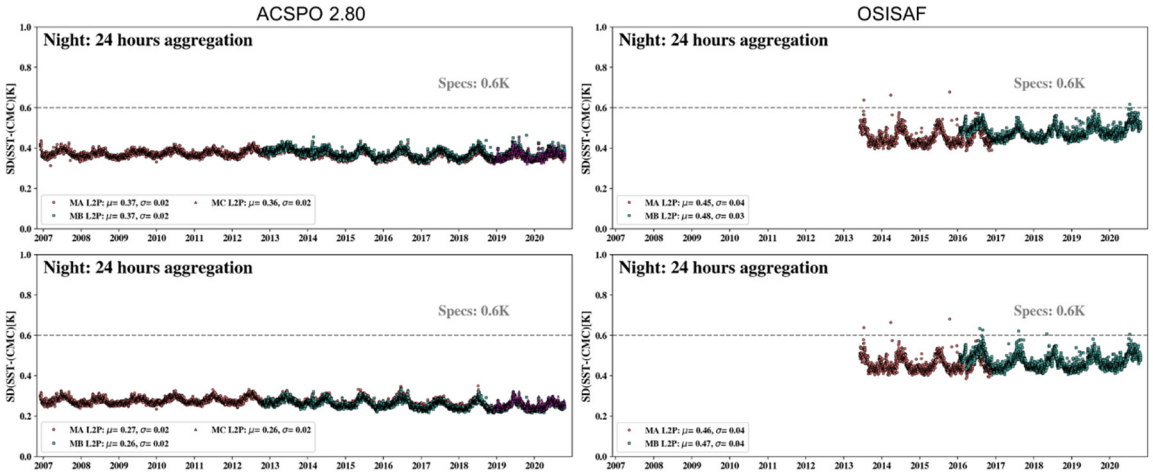

Figure 20. Time series of nighttime daily standard deviations of (top panels) 'subskin'– CMC SST and (bottom panels) 'debiased' – CMC L4 SST from (left panels) ACSPO and (right panels) OSISAF datasets.

5.1 Nighttime Time Series of Clear-Sky Ratio

Figure 21 (left panel) shows that nighttime ACSPO clear-sky fractions are consistent across all three platforms, at ~20-21% and show seasonality.

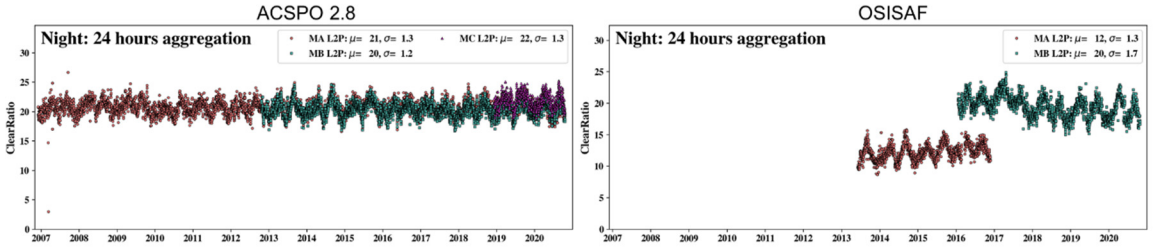

Figure 21. Time Series of nighttime Clear-Sky Ratio (Fraction of clear-sky pixels to all ocean ice-free pixels, in %) in the (left panel) ACSPO and (right panel) OSISAF datasets.

OSISAF clear-sky fractions (right panel) for Metop-B increased compared to Metop-A. The clear-sky fractions for Metop-B are on average close to ACSPO, but a little more variable in time. As in ACSPO, it also shows some seasonality.

The daytime clear-sky fractions for ACSPO are almost the same as the nighttime and can be seen at SQUAM [14].

6. OUTSTANDING ISSUES

Figure 22 shows the latitudinal Hovmöller diagrams of Metop-A and -B 'subskin' – CMC SST biases. The two most noticeable problems are (a) systematic warm biases in the Southern high latitudes, and cold biases in the Northern high latitudes; and (b) cold SST biases forming periodic "arcs" in the Northern hemisphere. Work is underway to understand the root cause of those, and fix when possible. The latter issue, in particular, is deemed to be due AVHRR calibration issues in the twilight parts of the nighttime orbit. It is currently being explored under the RAN2 AVHRR GAC project [30], and we plan to explore similar corrections for the AVHRR FRAC dataset.

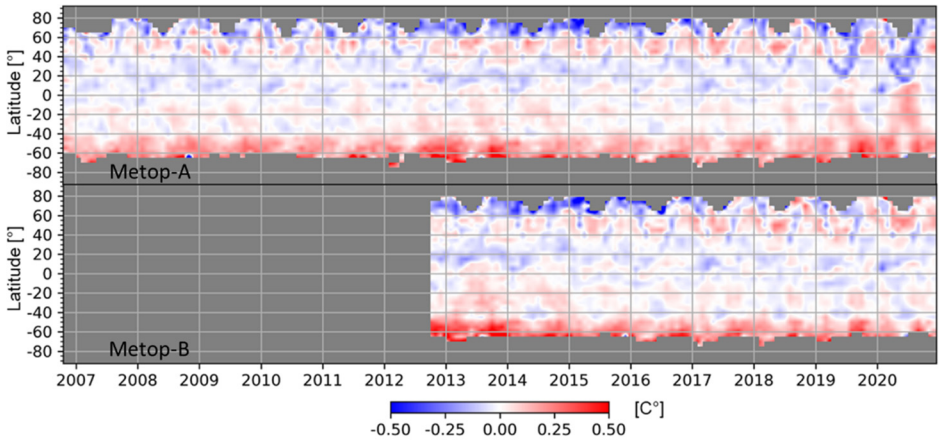

Figure 22. Nighttime Hovmöller diagrams of monthly latitudinal biases of ACSPO 'subskin' (GR) – (D+TM) SST for the (top panel) Metop-A and (bottom panel) Metop-B full missions.

7. SUMMARY

The first complete SST record from 1.1km AVHRR FRAC data onboard Metop-A, -B and -C has been created at NOAA with the Advanced Clear-Sky Processor for Oceans (ACSPO) system. The periods from the beginning of each mission to present were covered with the 1st historical reprocessing (Reanalysis-1, RAN1) and are continued with near-real time (NRT) processing of the current data. Special steps are taken to process NRT data maximally consistently with RAN1, given the lack of the right-hand side of the time scale in real time operations.

The stability of the validation statistics on time scales longer than 1 month, and their consistency between the three platforms, are ensured by daily recalculation of regression coefficients. In RAN1, the matchups for coefficient calculation are collected within time windows centered at the processed day. In NRT, the coefficients are derived from past windows" of the same size, but ending from 4 to 10 days before the processed day.

SSES bias correction in ACSPO reduces the variability of SST accuracy (global biases wrt quality controlled *in situ* data) and improves the precision (i.e., standard deviation) of fitting *in situ* SSTs.

The performance of the full records of the ACSPO AVHRR FRAC RAN1 SSTs from Metop-A (2006-pr), -B (2012-pr) and -C (2018-pr) are compared with SSTs retrieved at OSISAF from Metop-A (2013-2016) and -B (2016-pr). The ACSPO, in general, provides data with improved accuracy, stability and consistency of SST between the three platforms with respect to both drifting and tropical moored buoys and Argo floats, at a comparable or increased coverage, 20-21% of global ocean. The improvement in the global statistics is especially noticeable in 'debiased' SST.

The ongoing next stage of the Metop FRAC SST Reanalysis is the mitigation of the aforementioned AVHRR L1B calibration abnormalities to eliminate the cold anomalies in the northern hemisphere and improvement of the SST retrieval algorithm to eliminate remaining high latitude warm biases.

The full mission RAN1, complemented with NRT data, are being archived at PO.DAAC, and are also planned to be archived at the NOAA NCEI.

8. ACKNOWLEDGEMENT

The views, opinions, and findings in this report are those of the authors and should not be construed as an official NOAA or U.S. government position or policy.

REFERENCES

[1] Petrenko, B., Ignatov, A., Kihai, Y. *et al.*, "Clear-Sky Mask for the Advanced Clear-Sky Processor for Oceans," Journal of Atmospheric and Oceanic Technology, 27(10), 1609-1623 (2010).

[2] Ignatov, A., Zhou, X. J., Petrenko, B. *et al.*, "AVHRR GAC SST Reanalysis Version 1 (RAN1)," Remote Sensing, 8(4), (2016).

[3] Petrenko, B., Ignatov, A., Kihai, Y. *et al.*, "Sensor-Specific Error Statistics for SST in the Advanced Clear-Sky Processor for Oceans," Journal of Atmospheric and Oceanic Technology, 33(2), 345-359 (2016).
[4] Petrenko, B., Ignatov, A., Kihai, Y. *et al.*, "Evaluation and selection of SST regression algorithms for JPSS VIIRS," Journal of Geophysical Research-Atmospheres, 119(8), 4580-4599 (2014).
[5] Ignatov, A., Gladkova, I., Ding, Y. N. *et al.*, "JPSS VIIRS level 3 uncollated sea surface temperature product at NOAA," Journal of Applied Remote Sensing, 11, (2017).
[6] Jonasson, O., Gladkova, I., Ignatov, A. *et al.*, Progress with development of global gridded super-collated SST products from low Earth orbiting satellites (L3S-LEO) at NOAA SPIE, SI (2020).
[7] STAR, "GHRSST NOAA/STAR Metop-A AVHRR FRAC ACSPO v2.80 1km L2P Dataset (GDS v2)", DOI: 10.5067/GHMTA-2PS28: (2021).
[8] STAR, "GHRSST NOAA/STAR Metop-B AVHRR FRAC ACSPO v2.80 1km L2P Dataset (GDS v2)", DOI: 10.5067/GHMTB-2PS28: (2021).
[9] STAR, "GHRSST NOAA/STAR Metop-C AVHRR FRAC ACSPO v2.80 1km L2P Dataset (GDS v2)", DOI: 10.5067/GHMTC-2PS28: (2021).
[10] STAR, "GHRSST NOAA/STAR Metop-A AVHRR FRAC ACSPO v2.80 0.02º L3U Dataset (GDS v2)", DOI: 10.5067/GHMTA-3US28: (2021).
[11] STAR, "GHRSST NOAA/STAR Metop-B AVHRR FRAC ACSPO v2.80 0.02º L3U Dataset (GDS v2)", DOI: 10.5067/GHMTB-3US28: (2021).
[12] STAR, "GHRSST NOAA/STAR Metop-C AVHRR FRAC ACSPO v2.80 0.02º L3U Dataset (GDS v2)", DOI: 10.5067/GHMTC-3US28: (2021).
[13] Dash, P., Ignatov, A., Kihai, Y. *et al.*, "The SST Quality Monitor (SQUAM)," Journal of Atmospheric and Oceanic Technology, 27(11), 1899-1917 (2010).
[14] "SST Quality Monitor (SQUAM AVHRR FRAC)", https://www.star.nesdis.noaa.gov/socd/sst/squam/polar/avhrrfrac/.
[15] Xu, F., and Ignatov, A., "In situ SST Quality Monitor (iQuam)," Journal of Atmospheric and Oceanic Technology, 31(1), 164-180 (2014).
[16] "in situ SST Quality Monitor system (iQuam)", https://www.star.nesdis.noaa.gov/socd/sst/iquam/.
[17] Pryamitsyn, V., Ignatov, A., Petrenko, B. *et al.*, "Evaluation of the initial NOAA AVHRR GAC SST Reanalysis Version 2 (RAN2 B01)," Ocean Sensing and Monitoring Xii, 11420, (2020).
[18] Petrenko, B., Pryamitsyn, V., Ignatov, A. *et al.*, SST and cloud mask algorithms in reprocessing 1981-2002 NOAA AVHRR data for SST with the Advanced Clear-Sky Processor for Oceans (ACSPO) SPIE, SI (2020).
[19] He, K., Ignatov, A., Kihai, Y. *et al.*, "Sensor Stability for SST (3S): Toward Improved Long-Term Characterization of AVHRR Thermal Bands," Remote Sensing, 8(4), (2016).
[20] "3S Sensor Stability for SST v2.0", https://www.star.nesdis.noaa.gov/socd/sst/3s/.
[21] OSISAF, "GHRSST Level 2P sub-skin Sea Surface Temperature from the Advanced Very High Resolution Radiometer (AVHRR) on Metop satellites (currently Metop-A) (GDS V2) produced by OSI SAF" NASA Physical Oceanography DAAC, DOI: 10.5067/GHAMA-2PO02,https://podaac.jpl.nasa.gov/dataset/AVHRR_SST_METOP_A-OSISAF-L2P-v1.0/ (2015).
[22] OSISAF, "GHRSST Level 2P Global Subskin Sea Surface Temperature from the Advanced Very High Resolution Radiometer (AVHRR) on the MetOp-B satellite (GDS2 version)" NASA Physical Oceanography DAAC, DOI: 10.5067/GHAMB-2PO02,https://podaac.jpl.nasa.gov/dataset/AVHRR_SST_METOP_B-OSISAF-L2P-v1.0/ (2016).
[23] Le Borgne, P., Private communication.
[24] METEO FRANCE, "Product User Manual (PUM) for the Low Earth Orbiter Sea Surface Temperature", http://www.osi-saf.org/lml/doc/osisaf_cdop2_ss1_pum_leo_sst.pdf (2020).
[25] Saux Picart, S., "Algorithms Theoretical Basis Document for the Low Earth Orbiter Sea Surface Temperature Processing", http://www.osi-saf.org/lml/doc/osisaf_cdop3_ss1_atbd_leo_sst_1_3.pdf (2018).
[26] Le Borgne, P., Roquet, H., and Merchant, C. J., "Estimation of Sea Surface Temperature from the Spinning Enhanced Visible and Infrared Imager, improved using numerical weather prediction," Remote Sensing of Environment, 115(1), 55-65 (2011).
[27] Brasnett, B., and Colan, D. S., "Assimilating Retrievals of Sea Surface Temperature from VIIRS and AMSR2," Journal of Atmospheric and Oceanic Technology, 33(2), 361-375 (2016).

[28] CMC, "GHRSST Level 4 CMC0.2deg Global Foundation Sea Surface Temperature Analysis (GDS version 2)" NASA Physical Oceanography DAAC, 10.5067/GHCMC-4FM02,http://podaac.jpl.nasa.gov/dataset/CMC0.2deg-CMC-L4-GLOB-v2.0 (2012).
[29] CMC, "GHRSST Level 4 CMC0.1deg Global Foundation Sea Surface Temperature Analysis (GDS version 2)" NASA Physical Oceanography DAAC, 10.5067/GHCMC-4FM03,https://podaac.jpl.nasa.gov/dataset/CMC0.1deg-CMC-L4-GLOB-v3.0 (2017).
[30] Petrenko, B., Pryamitsyn, V., and Ignatov, A., Filtering cold outliers in SST retrieved from early AVHRRs during RAN2 AVHRR GAC SPIE, (2021).